Global Analysis of FPSO and Shuttle Tankers During Side-by-Side Offloading

by

B.J. Koo and M.H. Kim
Dept. of Civil Engineering (Ocean Engineering Program)
Texas A&M University

Final Project Report
Prepared for the Minerals Management Service
Under the MMS/OTRC Cooperative Research Agreement
1435-01-99-CA-31003
Task Order 73604
MMS Project Number 488

and

OTRC Industry Consortium

March, 2006

OTRC Library Number: 03/06A170

For more information contact:

Offshore Technology Research Center
Texas A&M University
1200 Mariner Drive
College Station, Texas 77845-3400
(979) 845-6000

or

Offshore Technology Research Center
The University of Texas at Austin
1 University Station C3700
Austin, Texas 78712-0318
(512) 471-6989

A National Science Foundation Graduated Engineering Research Center

TABLE OF CONTENTS

LIST OF TABLES AND FIGURES

Tables

Figures

Global Analysis of FPSO and Shuttle Tankers During Side-by-Side Offloading

B.J. Koo and M.H. Kim
Dept. of Civil Engineering (Ocean Engineering Program)
Texas A&M University
College Station, Texas 77843
m-kim3@tamu.edu

ABSTRACT

Multiple floating structures are being considered for a variety of offshore oil and gas projects. Examples include (1) FPSO and a shuttle tanker during loading; (2) LNG carriers and floating (or fixed) offshore unloading terminals; and floating mobile offshore drilling rigs (MODUs) and moored floating production systems (FPSs); and tender assisted drilling operations. The responses of each structure in the system can be influenced by interactions with the other structure(s), and the relative motion between the structures during operations is an important design and operational consideration. An analysis tool that can accurately and reliably predict the relative motions of multi-structure systems is needed. The analyses must consider the hulls of the floating structures, the mooring lines and any risers attached to each structure, and any interconnections between the structures (e.g., lines, umbilicals, yokes, and fenders). Few existing numerical models fully account for the complete hydrodynamic and line interactions between the coupled floating units. In this study, WINPOST was extended to be able to analyze the motions and interactions of an FPSO (or LNG Carrier) and a shuttle tanker during both side-by-side and tandem offloading scenarios.

The hydrodynamic interaction and mechanical coupling effects of two floating platforms connected by elastic lines are investigated by using a time-domain multi-hull/mooring/riser coupled dynamics analysis program. Particular attention is paid to the contribution of off-diagonal hydrodynamic interaction terms on the relative motions during side-by-side offloading operation. An exact method termed the Combined Matrix Method (CMM) was developed that includes all the vessel and line dynamics and the 12x12 hydro-dynamic coefficients in a combined matrix. The CMM method was compared with two typical approximation methods: the No Hydrodynamic Interaction (NHI) method which is an iteration method that does not consider the hydrodynamic interaction between two vessels; and the Separated Matrix Method (SMM) iteration method that partially considers the hydrodynamic interaction between two vessels that ignores the off-diagonal cross-coupling terms in 12x12 hydrodynamic coefficient matrix. Comparisons were made for a side-by-side offloading operation in two different environmental conditions. The numerical examples show that there is a significant discrepancy at sway and roll modes between the exact and the approximation methods, which means that the cross-coupling (off-diagonal block) terms of the full hydrodynamic coefficient matrix play an important role in the case of side-by-side offloading operation. Therefore, such approximation methods should be used with care. The fender reaction forces, which exhibit large force with contact but no force without contact, were also included in the time-domain simulation studies.

I. INTRODUCTION

As demands of oil and gas grow, field development with multiple floating platforms, which was considered to be very challenging in the past, becomes more and more common nowadays. One example is FPSO (Floating Production Storage and Offloading) offloading operation to shuttle tankers. Another example is the combination of TLP (Tension Leg Platform), drilling barge, and floating FSU (Floating Storage Unit). Recently, the demand of clean energy, such as LNG (Liquefied Natural Gas), rapidly grows, and near-shore or offshore floating LNG terminals have been proposed. In such a case, LNG carriers should be operated in the proximity of the terminal and the effects of hydrodynamic interactions have to be carefully taken into consideration for safe operation.

An FPSO production system that offloads oil to shuttle tankers can be much cheaper than installing new underwater pipelines in a remote deepwater oil and gas field. In such a case, the tandem offloading with floating hose is a common and safe practice. However, the offloading operation from LNG carrier to a LNG terminal should be done with great care since the flow lines have to overcome extremely low temperature, and the arrangement and the gap distance are restricted by the arm-length of LNG off-loading lines. The most feasible and economical practice seems to be the side-by-side offloading operation using conventional LNG off-loading lines. Therefore, the study of hydrodynamic interaction effects between the two large-volume floating bodies in close proximity should be an important element of the development, operation, and downtime analysis of floating-LNG-terminal system.

The hydrodynamic interactions between multiple bodies have been reported by many researchers; Ohkushu (1974), Kodan (1984), and Fang and Kim (1986) analyzed the hydrodynamic interaction by using 2D-like strip theory. Vanm Oortmerssen (1979) and Loken (1981) used the linear diffraction theory with constant panel method, while Choi and Hong (2002) employed a HOBEM(higher order boundary element method) to study three-dimensional hydrodynamic interactions between two vessels. Multiple-body interactions in time domain was studied by Buchner et al. (2001), Hong et al. (2003), Lee (2002), and Kim (2003). They calculated hydrodynamic coefficients from the frequency-domain linear diffraction program, and then utilized those coefficients in time-domain simulations. Hong et al.(2003) and compared the potential-based computation with their experimental results for two vessels in side-by-side offloading operation with small gap. The comparison of motions and drift forces including the free-surface elevation at the gap was reasonable. Similar comparison was also made by Kim (2003).

To evaluate the responses of multiple floating platforms connected by lines more accurately, there are additional aspects to be considered. The first aspect is mechanical coupling between the multi-bodies. Second, floating platforms possess many slender members, such as mooring lines, risers, and hawsers, and their coupling effects with hull should be carefully accounted for. In this research project, the hull/mooring/riser/hawser dynamic coupling effects as well as hydrodynamic interactions between two vessels are fully taken into consideration. In other

studies of FPSO-shuttle offloading operability, Sphier et al. (2000) and Lee and Choi (2000) used a set of simplified ship-maneuvering equations. However, this kind of much simpler approach may not be able to include all the complicated features of 2-body hydrodynamic interactions.

The dynamic coupling between hull and slender members can be evaluated in several different ways. One simple approach is called uncoupled analysis, which assumes that mooring lines, risers, and hawsers respond statically (as massless nonlinear springs) to hull motion, e.g. Lee (2002)). With this assumption, the inertia and damping effects as well as hydrodynamic loading on the slender members are not accounted for. When necessary, the mooring dynamics are evaluated separately as a post processing after obtaining the fairlead motions. The reliability and accuracy of this approach depend on platform-mooring types and water depth. Kim et al. (2001a and 2001b), and Ma et al. (2000) showed that such an uncoupled analysis of TLPs and spars may be inaccurate when used in deepwater. Wichers et al. (2001a and 2001b) showed that the uncoupled analysis may give even larger error in the case of an FPSO, and recommended the fully-coupled dynamic models to more reliably estimate realistic design values.

In the present paper, the side-by-side offloading operation from a turret-moored FPSO to hawser-connected shuttle tankers is investigated. The turret-moored weathervaning FPSOs are more difficult to analyze motions than spread-moored FPSOs due to the fact that they may undergo large yaw motions and wind-wave-current loads are generally sensitive to them. Therefore, to evaluate more reliably the responses of turret-moored FPSOs and shuttle tankers in wind, wave, and current, the effects of large yaw motion should be considered. Wichers (1988), Kim and Kim(2002) and Kim(2003), for example, included such effects. Arcandra et al.(2004) investigated such effects in more detail.

To verify the developed numerical simulation method, a series of large-scale experiments were conducted in the 3D Offshore Technology Research Center wave basin at Texas A&M University for a turret-moored FPSO designed for 6000-ft water depth. The numerically simulated FPSO global motions for non-parallel wind-wave-current environment were systematically compared with those measured from experiments. They were in good agreement as reported in Kim et al (2005). In the present study, the numerical analysis is further extended to two large vessels, for example an FPSO (or LNG Carrier) and a Shuttle Tanker operating in close proximity in side-by-side offloading operation.

The time domain hull/mooring /riser/hawser coupled dynamic analyses including two vessels were carried out by three different methods i.e. first, based on the exact Combined Full-Matrix Method (CMM) (Kim (2003); second, an iterative Separated-Matrix Method (SMM); and thirdly, No-Hydrodynamic-Interaction (NHI) method. Using the iterative separated matrix method, the hydrodynamic interactions are not fully captured but the corresponding module development can be greatly simplified and the resulting matrix size and computational time can be reduced by solving the individual vessels separately in an iterative manner. However, the reliability of such a simplified method has to be checked against the combined full matrix method. To the best of

authors' knowledge, this kind of comparison has not been published. The main objective of this study is to assess the performance of the three different approaches for side-by-side offloading operation with various environmental conditions. Finally, the effects of fender-induced contact loading are also numerically modeled and analyzed in a similar way as Koo et al. (2004), which is possible only in time-domain approach.

II. FORMULATION

Hydrodynamics of Multiple Floating Bodies in Time Domain Analysis

When a large three-dimensional body interacts with incident waves, the hydrodynamic coefficients and wave exciting forces and moments can be obtained by using the first- and second-order diffraction/radiation theory. In the diffraction/radiation theory, the total velocity potential can be decomposed into incident, diffraction, and radiation potentials. The total velocity potential satisfies the Laplace equation as a governing equation and all the requisite boundary conditions along the closed boundary including bottom, free surface, body boundary, and radiation boundary. The rigid-body motion of a single floating body can be described by 6-DOF (degree of freedom) motions. Therefore, for N multiple floating bodies, 6N-DOF motions have to be simultaneously solved i.e. one diffraction problem with all the body fixed and 6N radiation problems in which a motion is prescribed on one body while all the other bodies are fixed. Therefore, the interaction effects come from both the diffraction and radiation problems. In the present paper, the detailed hydrodynamic formulations for N bodies are not presented. Readers are directed to Kim (2003) for the details.

To obtain all the hydrodynamic coefficients of N bodies, such as added mass, radiation damping, first- and second-order wave-frequency and mean-drift forces, a three-dimensional second-order diffraction/radiation panel program WAMIT (Lee, 1999) was used. The computed frequency-domain hydrodynamic coefficients are used in the time-domain equation expressed by a two-term Volttera series expression via Kramers-Kronig relation. In the time-domain equation, the frequency-dependent radiation damping is included in the form of convolution integral (Ran, Kim). When computing the convolution integral of multiple bodies, the retardation function (Fourier cosine transform of the radiation damping) can be highly oscillatory and slowly decay, so special attention should be paid, as pointed out by Hong et al. (2003).

In the present case studies, the surge-sway-yaw natural frequencies are very small, thus only the second-order difference-frequency forces near the diagonal (mean-drift) of the QTF (Quadratic Transfer Function) are required, which justifies the use of the so-called Newman's approximation. It is shown in Kim (2003) that this simpler approach produces reasonable results in case of a turret-moored FPSO when compared with more accurate, time-consuming full-QTF method. In this paper, the Newman's approximation is employed for numerical examples. The wave drift damping was calculated by Aranha's formula for the same turret-moored FPSO, its

effects are found to be small (Arcandra, 2001), thus wave drift damping is not considered in this study.

To calculate the responses of N floating bodies, the equation of motion can be expressed as follows:

$$\begin{bmatrix} M_1 + m^a_{1,1}(\infty) & \cdots & m^a_{1,N}(\infty) \\ \vdots & & \vdots \\ m^a_{N,1}(\infty) & \cdots & M_N + m^a_{N,N}(\infty) \end{bmatrix} \begin{Bmatrix} \ddot{\vec{x}}_1 \\ \vdots \\ \ddot{\vec{x}}_N \end{Bmatrix} + \begin{bmatrix} \int R_{11}(t-\tau)d\tau & \cdots & \int R_{1,N}(t-\tau)d\tau \\ \vdots & & \vdots \\ \int R_{N,1}(t-\tau)d\tau & \cdots & \int R_{N,N}(t-\tau)d\tau \end{bmatrix} \begin{Bmatrix} \dot{\vec{x}}_1 \\ \vdots \\ \dot{\vec{x}}_N \end{Bmatrix} \quad (1)$$
$$+ \begin{bmatrix} K_1 & \cdots & \\ \vdots & \ddots & \\ & & K_{N,N} \end{bmatrix} \begin{Bmatrix} \vec{x}_1 \\ \vdots \\ \vec{x}_N \end{Bmatrix} = \begin{Bmatrix} \vec{F}_1 \\ \vdots \\ \vec{F}_N \end{Bmatrix}$$

where, [M] is 6 x 6 structure mass sub-matrix, [m] is added mass sub-matrix at infinite frequency, [R] is the retardation function sub-matrix, [K] is the hydrostatic restoring-coefficient sub-matrix, [x] is motion vector in group, and [F] is external force vector in group. The subscript represents the body number. The force vector includes wave-frequency exciting force, wind force, current force, and slowly varying wave drift force.

Mechanical Coupling between Multiple Floating Bodies and Slender Members

To analyze the coupled dynamics of multiple floating bodies with mooring lines, risers, and hawsers in the most accurate manner, a big combined matrix including all the rigid bodies and slender members and their interactions should be solved simultaneously as an integrated system. For the static/dynamic analyses of slender members, an extension of the theory developed by Garrett (1982) was used. The methodology for the coupled dynamics of multiple floating platforms including slender members is in general similar to that of a single body (Koo et al., 2004), which is briefly summarized in the following.

Assuming no torque or external twisting moment, one can derive the linear momentum-conservation equation with respect to a position vector $\vec{r}(s,t)$ that is a function of arc length (s) and time (t):

$$-(B\vec{r}'')''+(\lambda\vec{r}')'+\vec{q} = m\ddot{\vec{r}} \quad (2)$$

$$\lambda = T - B\kappa^2 \quad (3)$$

$$T = T_0 + P_e A_e - P_i A_i \quad (4)$$

where prime and dot denote spatial and time derivatives, respectively, *B=EI (E=Young's modulus, I=sectional moment of inertia)* is bending stiffness, *T* the local effective tension, κ the local curvature, *m* the mass per unit length, $\vec{q}$ the distributed force on the rod per unit length, T_0 the local tension, P_e the external pressures, P_i the internal pressures, A_e and A_i are external and internal cross sectional areas. The scalar variable λ can be regarded as a Lagrange multiplier.

If the rod is assumed to be inextensible, the following condition must be satisfied;

$$\vec{r}' \cdot \vec{r}' - 1 = 0 \tag{5}$$

If the rod is extensible, the condition is more generalized to

$$\frac{1}{2}(\vec{r}' \cdot \vec{r}' - 1) = \frac{T}{A_t E} \approx \frac{\lambda}{A_t E} \tag{6}$$

$$A_t = A_e - A_i \tag{7}$$

For these equations, the geometric nonlinearity is fully considered and there is no special assumption made concerning the shape or orientation of the mooring line, as long as the rod remains elastic. The benefit of this equation is that (2) is directly defined in the global coordinate system and does not require any transformations to the local coordinate system. The normal component of the distributed external force on the rod per unit length, q_n, is given by the generalized Morison equation, (e.g. Paulling and Webster, 1986).

$$q_n = C_I \rho A_e \dot{v}_n + \frac{1}{2} C_D \rho D |v_{nr}| v_{nr} + C_m \rho A_e \ddot{r}_n \tag{8}$$

where C_I ,C_D and C_m are inertia, drag and added mass coefficients, and $\dot{v}_n$, v_{nr} and $\ddot{r}_n$ are normal fluid acceleration, normal relative velocity, and normal structure acceleration, respectively. The symbols ρ and *D* are fluid density and local diameter. In addition, the effective weight, or net buoyancy, of the rod should be included in q_n as a static load.

To develop the finite element formulation, consider a single element of length *L*, and use the following expression;

$$\vec{r}(s,t) = \sum_i A_i(s)\vec{U}_i(t) \tag{9}$$

$$\lambda(s,t) = \sum_m P_m(s)\lambda_m(t) \tag{10}$$

where A_i and P_m are interpolation function defined on the interval $0 \le s \le L$. Using equation (9) and (10), equation (2) can be reduced to the following equation by the Galerkin method and integration by parts (Garrett, 1982):

$$\int_0^L \left[B\vec{r}'' A_i'' + \lambda \vec{r}' A_i' - \vec{q} A_i + m\ddot{\vec{r}} A_i \right] ds = B\vec{r}'' A_i' \Big|_0^L + \left\{ \lambda \vec{r}' - \left(B\vec{r}'' \right)' \right\} A_i \Big|_0^L \tag{11}$$

where it is assumed that the shape function A_i is continuous on the element. The first boundary term of the right-hand side is related to the moments on the ends, and the second term is the force on the ends, i.e. they are natural boundary conditions. If equation (6) is used, we obtain:

$$\int_0^L P_m \left\{ \frac{1}{2}\left(\vec{r}' \cdot \vec{r}' - 1\right) - \frac{\lambda}{A_i E} \right\} ds = 0 \tag{12}$$

The position vector, its tangent, and the Lagrange multiplier are selected to be continuous at a node between adjacent elements. The interpolation functions A_i and P_m are chosen to be Hermitian cubic and quadratic functions of s as follows;

$$A_1 = 1 - 3\xi^2 + 2\xi^3,\ A_2 = \xi - 2\xi^2 + \xi^3,\ A_3 = 3\xi^2 - 2\xi^3,\ A_4 = -\xi^2 + \xi^3 \tag{13}$$

$$P_1 = 1 - 3\xi + 2\xi^2,\ P_2 = 4\xi(1-\xi),\ P_2 = \xi(2\xi - 1) \tag{14}$$

where $\xi = s/L$. The parameters $\vec{U}$ and λ are thus:

$$\vec{U}_1 = \vec{r}(0,t),\ \vec{U}_2 = L\vec{r}'(0,t),\ \vec{U}_3 = \vec{r}(L,t),\ \vec{U}_4 = L\vec{r}'(L,t) \tag{15}$$

$$\lambda_1 = \lambda(0,t),\ \lambda_2 = \lambda(L/2,t),\ \lambda_3 = \lambda(L,t) \tag{16}$$

Elements are combined using the continuity of $\vec{r}$, $\vec{r}'$ and λ. The natural boundary conditions at joint cancel out, leaving those conditions applicable at the ends of the rod. The ends of lines are connected to the hull through a generalized elastic(both linear and rotational) spring that can also model both fixed and hinged conditions at its extreme limit. The forces and moments proportional to the relative displacements are transmitted to the hull at the connection points. The transmitted forces from mooring lines to the platform are given by

$$\tilde{F}_P = \tilde{K}(\tilde{T}\tilde{u}_p - \tilde{u}_I) + \tilde{C}(\tilde{T}\dot{\tilde{u}}_p - \dot{\tilde{u}}_I) \tag{17}$$

where $\tilde{K}$ is the stiffness matrix, $\tilde{C}$ the damping matrix, $\tilde{T}$ the transformation matrix between the platform origin and connection point, $\tilde{u}_p$ and $\tilde{u}_I$ are displacement vectors of the platform and connection point.

The hull response equation is combined into the mooring-line equation in the time domain as follows;

$$(\tilde{M} + \tilde{M}_a(\infty))\ddot{\tilde{u}}_p + \int_0^\infty \tilde{R}(t-\tau)\dot{\tilde{u}}_p d\tau + \tilde{K}_H \tilde{u}_p = \tilde{F}_D + \tilde{F}^{(1)} + \tilde{F}^{(2)} + \tilde{F}_p + \tilde{F}_{WD} \tag{18}$$

where, $\tilde{M}$ and $\tilde{M}_a$ are structure mass and added mass, $\tilde{R}$ the retardation function (inverse cosine Fourier transform of radiation damping), $\tilde{K}_H$ the hydrostatic restoring coefficients, $\tilde{F}_D$ the drag force matrix on the hull, $\tilde{F}^{(1)}, \tilde{F}^{(2)}$ the first- and second-order wave load matrix on the hull, $\tilde{F}_p$ the transmitted force matrix from the interface and $\tilde{F}_{WD}$ the wave drift damping force matrix. The added mass at infinite frequency is obtained from Kramers-Kroing relation. For the time series of

$\tilde{F}^{(1)}, \tilde{F}^{(2)}$ and $\tilde{F}_{WD}$, a two-term Volterra series is used. From above time domain equation of motion, the hull/mooring line/riser coupled analysis can be achieved.

In the static analysis of mooring lines and risers, Newton's iteration method was used. Thus, the coupled force on the mooring at $(n+1)^{th}$ iteration can be approximated by the rule at $(n)^{th}$ iteration.

$$N_i^{(n+1)} = N_i^{(n)} + \frac{\partial N_i}{\partial r_j}\Delta r_j + \frac{\partial N_i}{\partial X_j}\Delta X_j + \frac{\partial N_i}{\partial \theta_j}\Delta \theta_j \tag{19}$$

Similarly, the coupled force on the platform at $(n+1)^{th}$ iteration can be approximated by:

$$F_i^{(n+1)} = F_i^{(n)} + \frac{\partial F_i}{\partial r_j}\Delta r_j + \frac{\partial F_i}{\partial X_j}\Delta X_j + \frac{\partial F_i}{\partial \theta_j}\Delta \theta_j \tag{20}$$

$$M_i^{(n+1)} = M_i^{(n)} + \frac{\partial M_i}{\partial r_j}\Delta r_j + \frac{\partial M_i}{\partial X_j}\Delta X_j + \frac{\partial M_i}{\partial \theta_j}\Delta \theta_j \tag{21}$$

Equation (19) shows that the mooring at the connecting node is coupled with the unknown platform motion. The second terms in the right hand side of Eq. (19), (20), and (21) are included in the equation of the mooring element which is coupled with the platform, while the third and fourth terms in the Eq. (19), (20), and (21) are included in the equation of the platform. The mooring and platform are coupled by the third and fourth terms of Eq. (19) and the second term of Eq. (20) and (21). The coupled force vectors, $N_i^{(n)}$, $F_i^{(n)}$ and $M_i^{(n)}$, are added to the force vectors at the right-hand side of the equations of the mooring element and the platform. At each iteration, the coupled algebraic equations are solved to obtain the solutions simultaneously. The iteration continues until a specific tolerance is reached.

In the time-domain integration, the coupled force on the mooring is added to the equations of mooring and platform motions and is integrated from time $t^{(n)}$ to $t^{(n+1)}$:

$$\int_{t^{(n)}}^{t^{(n+1)}} N_i dt = \frac{\Delta t}{2}\left(N_i^{(n+1)} + N_i^{(n)}\right) \approx \frac{\Delta t}{2}\left(\frac{\partial N_i}{\partial r_j}\Delta r_j + \frac{\partial N_i}{\partial X_j}\Delta X_j + \frac{\partial N_i}{\partial \theta_j}\Delta \theta_j + 2N_i^{(n)}\right) \tag{22}$$

$$\int_{t^{(n)}}^{t^{(n+1)}} F_i dt = \frac{\Delta t}{2}\left(F_i^{(n+1)} + F_i^{(n)}\right) \approx \frac{\Delta t}{2}\left(\frac{\partial F_i}{\partial r_j}\Delta r_j + \frac{\partial F_i}{\partial X_j}\Delta X_j + \frac{\partial F_i}{\partial \theta_j}\Delta \theta_j + 2F_i^{(n)}\right) \tag{23}$$

$$\int_{t^{(n)}}^{t^{(n+1)}} M_i dt = \frac{\Delta t}{2}\left(M_i^{(n+1)} + M_i^{(n)}\right) \approx \frac{\Delta t}{2}\left(\frac{\partial M_i}{\partial r_j}\Delta r_j + \frac{\partial M_i}{\partial X_j}\Delta X_j + \frac{\partial M_i}{\partial \theta_j}\Delta \theta_j + 2M_i^{(n)}\right) \tag{24}$$

Like the static analysis, the coefficients in the above equations go to the time-domain equations of the platform and the element of the mooring coupled with the platform.

CMM vs. SMM

The multi-body coupled analysis can be done by assembling the global matrix that includes all the hydrodynamic and mechanical coupling effects between vessels and slender members. In this study, two different methods are used in assembling the global matrix. The first method is CMM (combined matrix method). In this method, all the hydrodynamic coefficients and mechanical coupling of hull and slender members are included in one large matrix. This method in principle exactly accounts for all the hydrodynamic and mechanical interactions. The second method is SMM (separated matrix method). In this method, the global matrix is set up for each floating body and the mechanical coupling between the two vessels is calculated through the tension of hawser lines until convergence is achieved. The hawser lines are generally in the air and their length is short compared to mooring lines and risers, thus the inertia and damping effects from the hawsers are expected to be very small. The SMM can represent the mechanical coupling correctly but it cannot include the full hydrodynamic interactions. The major difference between the CMM and SMM occurs in the off-diagonal 6x6 added mass matrix and radiation damping matrix. Due to the separate global matrix set for each body, the SMM cannot consider the off-diagonal hydrodynamic interaction terms.

The global matrix formulations are illustrated in Fig. 1 and Fig. 2, in which the sub-matrix K_M represents the coefficients for mooring lines and risers, sub-matrix K_H represents the coefficients for hawser, sub-matrix K^C_{MP} and K^C_H represent coupling coefficients between hull and slender members, and sub-matrix K_P represents the coefficients for hull. The superscript in K_P matrix represents body number. The vectors U and F represent displacements and forces of hull and slender members.

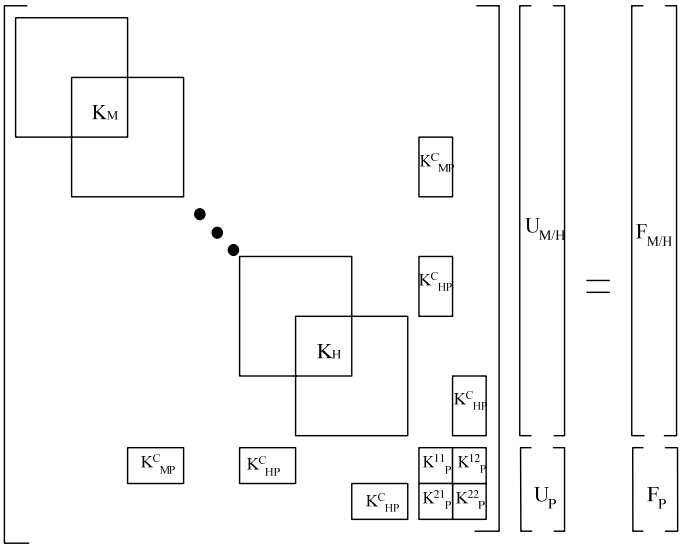

Fig 1. Global matrix of CMM(combined matrix method) (example for two bodies)

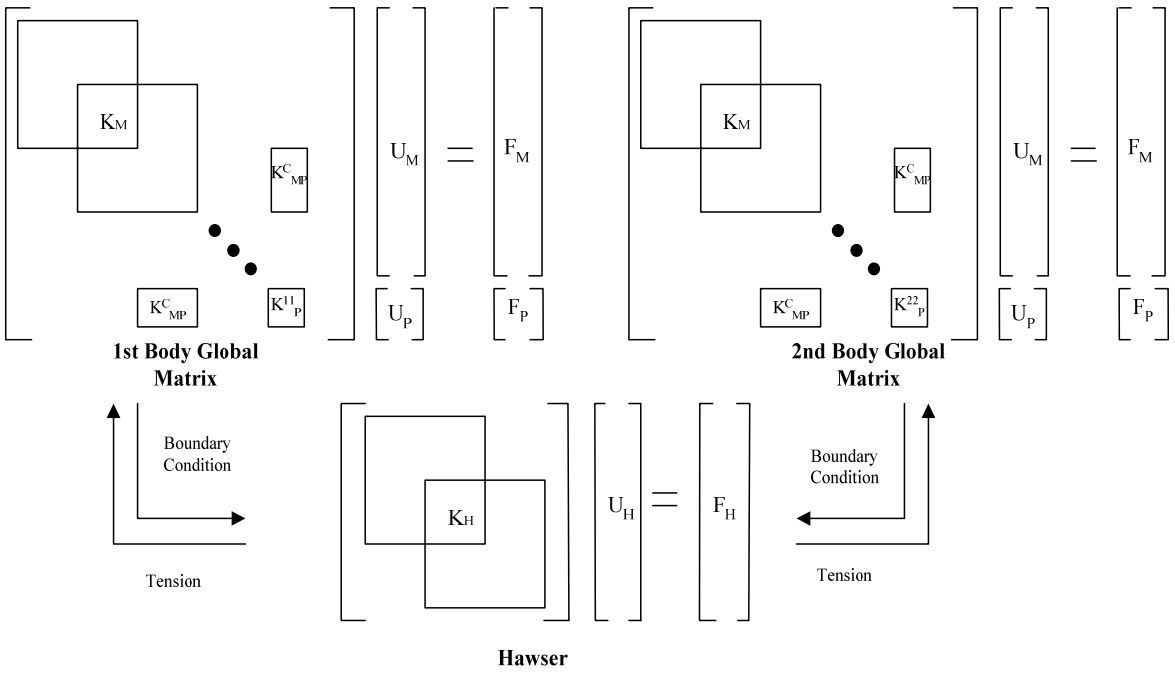

Fig 2. Global matrix of SMM(separated matrix method) (example for two bodies)

As illustrated in Fig. 1, the combined matrix method includes all the vessels and lines in one large matrix and the global matrix is inverted in every time step. Fig. 2 shows that the separated matrix method sets up the global matrix for each body and their mechanical interactions through hawsers are solved by iteration. At each time step and iteration, the body positions are given as essential boundary conditions of the hawser end points, while the hawser tension is given to each body as external forces. Due to the separation of global matrix, the off-diagonal (6x6) hydrodynamic interaction coefficients cannot be included in each separated matrix (i.e. $K^{12}{}_P$ and $K^{21}{}_P$ in Figure 1). Thus, the combined matrix method is the most accurate way to calculate the multiple-floating-body interactions. However, the matrix size of CMM increases in proportion to the number of vessels and slender members, which results in much longer computational time. Furthermore, when more than three floating bodies are involved, it is much more straight-forward to use SMM in the module development of the computer program. Under this circumstance, an important question is “how good is the SMM?” The importance of the off-diagonal (6x6) hydrodynamic interaction coefficients varies with the arrangement and distance of two vessels. It also depends on system characteristics and environmental conditions. When hydrodynamic interaction effects are expected to be smaller than mechanical coupling effects (e.g. tandem arrangement), the SMM can be an efficient way to solve the multi-body problem (Koo and Kim 2005).

Fender Effects In Time Domain Simulation

In general, there are fenders between LNG FPSO/terminal and LNG carrier in side-by-side offloading arrangement. The function of the fender is to prevent collision between the two

floating vessels. When the relative distance between LNG terminal and carrier is smaller than fender length (in the present study, initial gap), the fender exerts reaction forces on both bodies. Whereas, when the relative distance is greater than the fender length, there exist no reaction forces on both bodies. Therefore, a proper tender-reaction-force modeling is only possible in the time-domain analysis. In the present numerical simulation, the fenders are modeled as piecewise-linear gap springs for simplicity. Figure 3 shows the force-displacement curve for the fender. Note that the fender produces equal and opposite reaction forces on both bodies only when it is compressed.

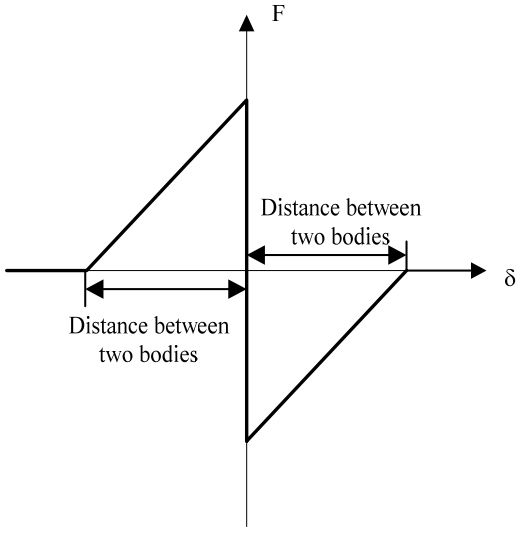

Figure 3. Force displacement curve for the fender

The effects of the fender can be expressed as follows:

when, $\left|\left(X_2^1 + P_2^1 + \theta_1^1 P_3^1 - \theta_3^1 P_2^1\right) - \left(X_2^2 + P_2^2 + \theta_1^2 P_3^2 - \theta_3^2 P_1^2\right)\right| \geq \Delta_2$ then

$$N_2 = 0 \tag{25}$$

when, $\left|\left(X_2^1 + P_2^1 + \theta_1^1 P_3^1 - \theta_3^1 P_2^1\right) - \left(X_2^2 + P_2^2 + \theta_1^2 P_3^2 - \theta_3^2 P_1^2\right)\right| < \Delta_2$

and $\left(X_2^1 + P_2^1 + \theta_1^1 P_3^1 - \theta_3^1 P_2^1\right) - \left(X_2^2 + P_2^2 + \theta_1^2 P_3^2 - \theta_3^2 P_1^2\right) < 0$ then

$$N_2 = K\left\{\left[\left(X_2^1 + P_2^1 + \theta_1^1 P_3^1 - \theta_3^1 P_2^1\right) - \left(X_2^2 + P_2^2 + \theta_1^2 P_3^2 - \theta_3^2 P_1^2\right)\right] + \Delta_2\right\} \tag{26}$$

and $\left(X_2^1 + P_2^1 + \theta_1^1 P_3^1 - \theta_3^1 P_2^1\right) - \left(X_2^2 + P_2^2 + \theta_1^2 P_3^2 - \theta_3^2 P_1^2\right) > 0$ then

$$N_2 = K\left\{\left[\left(X_2^1 + P_2^1 + \theta_1^1 P_3^1 - \theta_3^1 P_2^1\right) - \left(X_2^2 + P_2^2 + \theta_1^2 P_3^2 - \theta_3^2 P_1^2\right)\right] - \Delta_2\right\} \tag{27}$$

where, N is the reaction force from fender, K is the spring constant, X is the translational motion of the rigid body, P is the position vector of the location of fender with respect to the local

coordinate of the rigid body, θ is the angular motions of the rigid body, and Δ is the initial gap between the two floating bodies. The subscript represents the direction of rigid-body motions and superscript represents rigid-body number.

The fender forces and moments on the first body and the second body can be expressed as follows:

$$\vec{F}^1 = -\vec{N} \tag{28}$$

$$\vec{F}^2 = \vec{N} \tag{29}$$

$$\vec{M}^1 = \vec{P} \times -\vec{N} \tag{30}$$

$$\vec{M}^2 = \vec{P} \times \vec{N} \tag{31}$$

where, $\vec{F}$ is external force on the rigid body, $\vec{N}$ is the force from fender, $\vec{M}$ is the external moment on the rigid body. The fender force is calculated from the relative displacement between the two floating bodies.

III. NUMERICAL RESULTS AND DISCUSSIONS: Case Studies

The specifications of the FPSO/LNG and LNG carrier used in the present study are summarized in Table 1. The FPSO/LNG originally has 12 chain-polyester-chain mooring lines and 13 steel catenary risers. There are four groups of mooring lines, each group consists of 3 lines 5-degrees apart. Each mooring line has a studless chain at both ends. The effects of tangential drag on mooring lines and Coulomb friction from seabed were expected to be unimportant, and thus not included in this study. For simplicity, four equivalent mooring lines and one equivalent riser were used in the present simulations, with each equivalent line representing the combined effects of 3 mooring lines. The equivalent diameter was derived from the condition of 'equal drag force'. Table 2 shows the main particulars and hydrodynamic coefficients of mooring lines, risers, and hawsers. The water depth is 6000ft (1828 m).

Numerical simulations are conducted for the case of side-by-side offloading operation with 5-m gap for two different environmental conditions. Only the collinear wind-wave-current environmental conditions from the head direction are studied here. Fig. 4 shows the distribution of panels on LNG/FPSO and LNG carrier. Fig. 5 illustrates the mooring system, hawser connection, and environmental directions. The hawser connection is simplified compared to more realistic and complicated one. The two environmental conditions are tabulated in Table 3. Fig.6 illustrates the API wind spectrum used in the present simulation. As for the current and wind loading on the two vessels, the standardized OCIMF data sets (REF) are used.

The second-order slowly-varying wave forces are calculated from the so-called 'Newman's approximation'. In other words, the off-diagonal components of the difference-frequency wave-force QTF(quadratic transfer function) are approximated by the diagonal (mean-drift) values. This approximation is valid when the natural frequencies of slowly-varying motions are small, as

in the present case. The Newman's approximation may not be very reliable in the case of shallow water. The wave drift damping is expected to be small compared to other drag components, thus not included here (Arcandra, 2001). The same hull damping as in Kim et al (2005) is used.

Table 1:Main particulars of the turret-moored FPSO (or LNG carrier) and shuttle tanker used for simulation

Designation	Unit	FPSO (or LNG carrier)	Shuttle
Length LPP	m	310.00	248.00
Breadth	m	47.17	37.74
Draft	m	18.90	15.12
Displacement	m^3	240869.00	123324.93
Water plane area	m^2	13400.00	8576.00
Center of gavity above keel	m	13.32	10.66
Transverse radius of gyration	m	15.79	12.63
Longitudinal radius of gyration	m	115.03	92.02
Yaw radius of gyration	m	116.13	92.91
Wind area frontal	m^2	1012.00	647.68
Wind area side	m^2	3772.00	2414.08
Turret center line behind FPP	m	63.55	N/A

Table 2:Main particulars and hydrodynamic coefficients of mooring system, riser, and hawser.

Designation	Unit	Mooring Line Segment 1: chain	Segment 2: wire	Segment 3 : chain	Riser	Hawser
Pretension	kN	1.74E+03	1.74E+03	1.74E+03	1.14E+05	8.00E+05
Length at anchor point	m	9.14E+02	1.13E+03	9.14E+02	1.81E+03	N/A
Diameter	mm	8.17E+02	6.93E+02	8.17E+02	2.76E+03	N/A
Dry weight	kg/m	5.68E+02	5.16E+01	5.68E+02	2.56E+03	2.89E+01
Wet weight	kg/m	4.94E+02	1.35E+01	4.94E+02	1.31E+03	N/A
Stiffness AE	kN	2.73E+06	5.60E+05	2.73E+06	1.69E+08	1.87E+06
Inertia normal C		2.00	1.12	2.00	1.00	N/A
Drag normal Cd		2.45	1.20	2.45	1.00	N/A

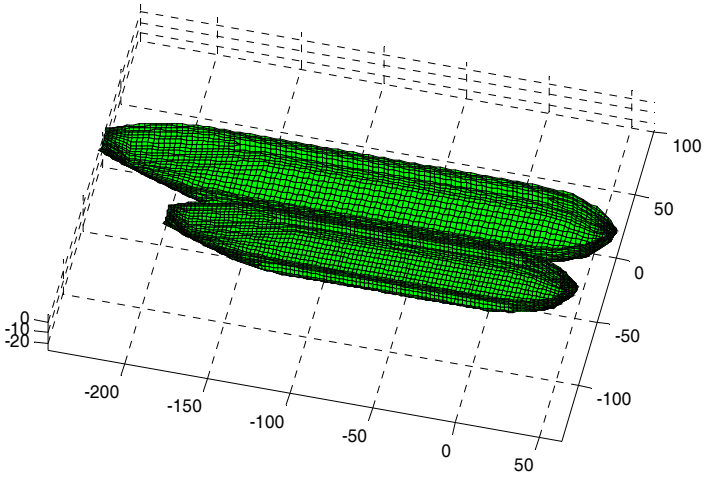

Fig. 4. Mesh generation of side-by-side moored FPSO (or LNG Carrier) and Shuttle.

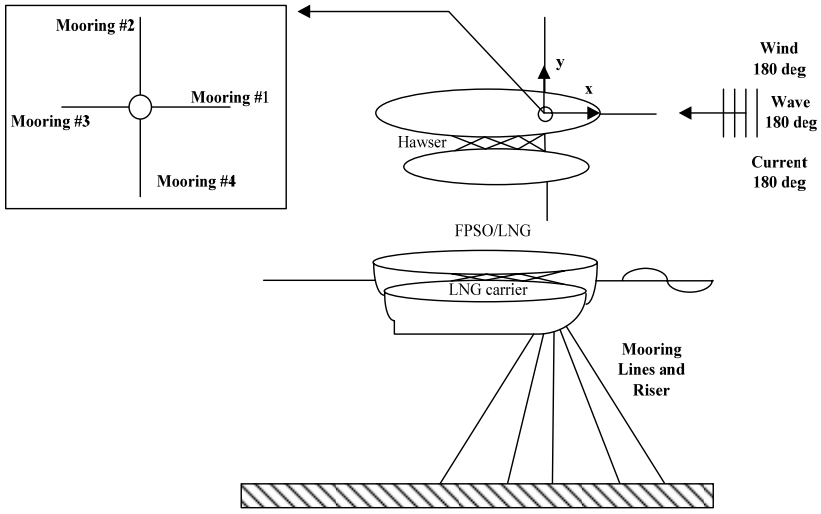

Fig. 5. Arrangement of mooring system, riser and hawser for side by side moored FPSO (or LNG Carrier) and Shuttle.

Table 3: Environmental condition for side by side moored FPSO (or LNG Carrier) and Shuttle

Wave (JONSWAP)		Quantities	Wind (API)	Quantities	Current(m/s)	Quantities
	Hs (m)	3.0	V_{10} (m/s)	5.0	Free surface	0.15
	Direction (deg)	180.0	Direction (deg)	180.0	at 60.96 m	0.15
					at 91.44m	0.50
CASE 1	Tp (sec)	16.5				
	Gamma	6.0				
CASE 2	Tp (sec)	8.3				
	Gamma	1.0				

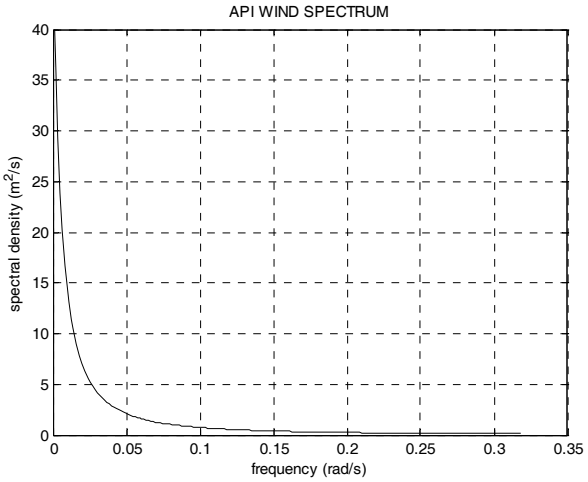

Fig. 6. API wind spectrum (at 10m above MWL, V_{10} = 5.0 m/s)

Side-by-side moored FPSO (or LNG Carrier) and Shuttle

As mentioned earlier, the hydrodynamic interactions between two side-by-side-moored vessels are studied by several researchers (e.g. Huijsmans et al. (2001), Buchner et al. (2001), Kim et al. (2003), and Hong et al. (2003)). Their results show that the sway motions of the two vessels are much larger than the single-body case in head sea condition. To better understand the characteristics of the hydrodynamic interaction between two vessels, the hydrodynamic coefficients for 5-m gap are presented in Fig. 7-8. Each figure shows the hydrodynamic coefficients of LNG/FPSO and LNG carrier for comparison. It is interesting to notice that, near a particular frequency (i.e. 0.7rad/s), the computed added mass and wave exciting force exhibit sharp variation. It can be explained by the pumping-mode resonance of a water column between the two bodies. Near the Helmholtz pumping resonance, the added mass can be negative. In the head sea condition, the sway-force and roll-moment of a single body should vanish due to symmetry. However, in the two-body case, their magnitudes are appreciable as a result of hydrodynamic interactions.

To evaluate the hydrodynamic interaction effects on FPSO (or LNG Carrier) and Shuttle, two environmental conditions are considered. The respective wave amplitude spectra are shown in

Fig.9-10. To assess the acceptability of different levels of approximation methods common in offshore industry, three different approaches are compared.

(1) No Hydrodynamic Interaction: hydrodynamic coefficients of respective single bodies are used.

(2) SMM: Iterative method using separated matrices ignoring the off-diagonal 6x6 blocks in 12x12 hydrodynamic-coefficient matrix.

(3) CMM: Combined (whole) matrix method including all 12x12 hydrodynamic-coefficient matrix

The simulation results for CASE 1 environmental condition are shown in Fig.11-13 and Table 4-6. The most conspicuous discrepancy among the three different methods occurs in sway and roll. If the two-body hydrodynamic interaction effects are not included at all (Fig.11), the sway and roll motions are significantly underestimated. The FPSO (or LNG Carrier) sway motion by CMM (Fig.13), which includes all the interaction effects, is larger than that of SMM(Fig.12). It means that the off-diagonal blocks in 12x12 hydrodynamic-coefficient matrix play an important role and should not be neglected in the present case. To confirm this statement, an additional simulation is conducted by CMM with zero off-diagonal 6x6 hydrodynamic interaction coefficients. The result (called SCMM) turns out to be the same as that of SMM, as expected. This test also independently verifies the correctness of the SMM coding.

As can be seen in Table 4, the SMM under-predicts the FPSO (or LNG Carrier) sway rms by 42% (wave-frequency component by 55% and low-frequency component by 7%). On the other hand, SMM over-predicts the Shuttle roll rms by 112%. The discrepancy of the shapes of the sway spectra of LNG-FPSO among the three methods is also noticeable. In CMM, wave frequency components are greater than low-frequency components. The opposite trend holds true in SMM and NHI cases. In Fig.11, wave-frequency sway and roll responses are very small neglecting the hydrodynamic interaction effects, as can also be seen in Fig.14.

To see the discrepancies more clearly among the three different approaches, sway RAOs are obtained in Fig. 14 from the square-root of the ratio of the response spectrum to wave spectrum. It is already mentioned that the SMM and SCMM are not differentiable. For the FPSO (or LNG Carrier) sway RAOs, the SMM (dashed line) significantly underestimates the actual motion of CMM (solid line) especially near 0.38 rad/s. On the other hand, SMM overestimates the actual FPSO (or LNG Carrier) sway motion over the range 0.6-0.9 rad/sec (including Helmholtz resonance frequency). As for Shuttle sway motion, SMM significantly over-predicts near 0.56 rad/s.

Fig 15 shows the time histories of relative sway motions between the two vessels. Compared to more accurate solution CMM, the SMM under-predicts the relative sway rms by 43% (see Table 5). Figs.16 show the mooring-line top-tension spectra of Case 1 calculated by CMM and SMM.

The mooring lines position the FPSO (or LNG Carrier),, and are most influenced by its motion. The SMM tends to over-predict the top tension on taut line 1 and slack line 3. The taut-side mooring tension is basically quasi-static and mainly depends on slowly-varying surge motions. The surge motion spectra clearly show that the SMM overestimates both the wave-frequency and low-frequency FPSO (or LNG Carrier) surge motions. In the slack mooring line, the dynamic effects by wave-frequency motions are significant.

Figs. 17 show the spectra of hawser #1 top tension and fender #1 force. The fender-force spectra clearly show the trend of under-prediction (rms by 32%) by SMM due to smaller relative sway motions (Fig.15). On the other hand, the wave-frequency hawser top tension is overestimated (rms by 12%) by SMM. The reason is that the fender forces are modeled to act against only the relative sway motion but the hawsers are influenced by both surge and sway relative motions due to its cross (X) arrangement (see Fig.5).

Fig. 18 shows fender-force time series. When the relative sway motion is smaller than the initial gap 5m (negative), the fender pushes FPSO (or LNG Carrier) and Shuttle to the opposite direction. On the other hand, when the relative sway is greater than the initial gap(positive), no force is acting on the fenders of FPSO (or LNG Carrier) and Shuttle. In the present analysis, the possible Coulomb friction between the fenders of two vessels in the surge direction is not considered. Since the fender reaction force is idealized as two springs, the resulting reaction force is not impact-like but rather gradual. The more realistic impact-like results can be obtained by using quadratic or cubic force-displacement curves, as pointed out in Koo et al. (2004). Table 7 summarizes the mooring and hawser top tension and fender force acting on FPSO (or LNG Carrier).

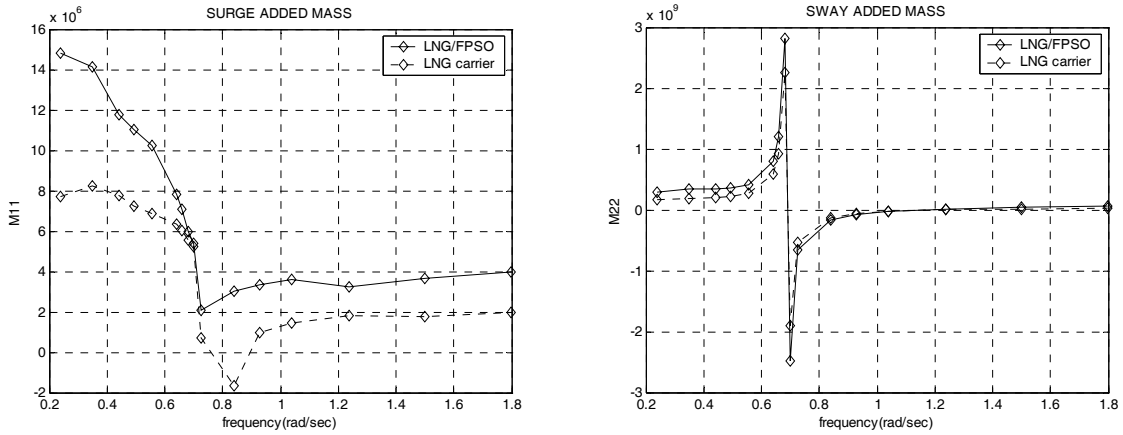

Fig. 7 Added mass of FPSO (or LNG Carrier) and Shuttle for 5-m gap

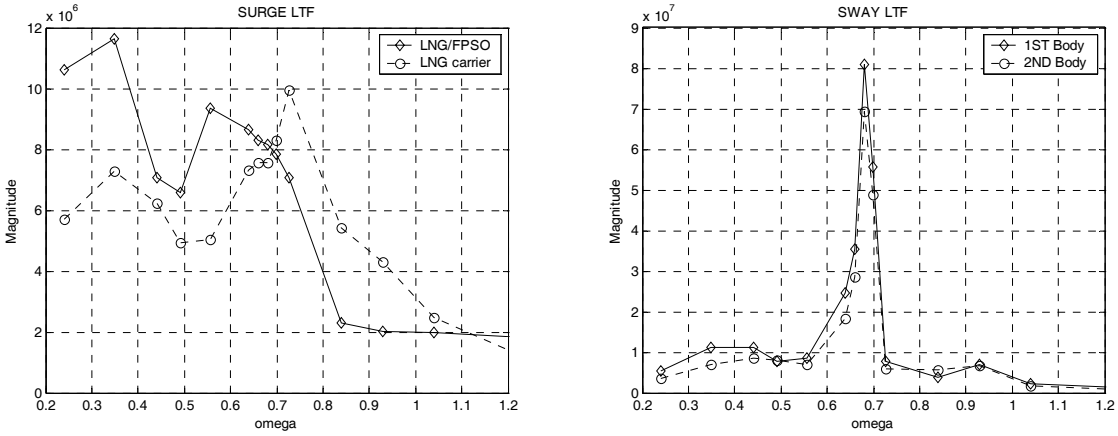

Fig. 8 Linear wave-force transfer function of FPSO (or LNG Carrier) and Shuttle for 5-m gap

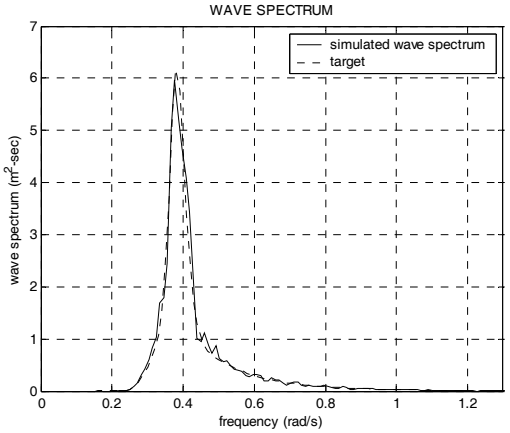

Fig. 9 Wave amplitude spectrum (side by side Case 1)

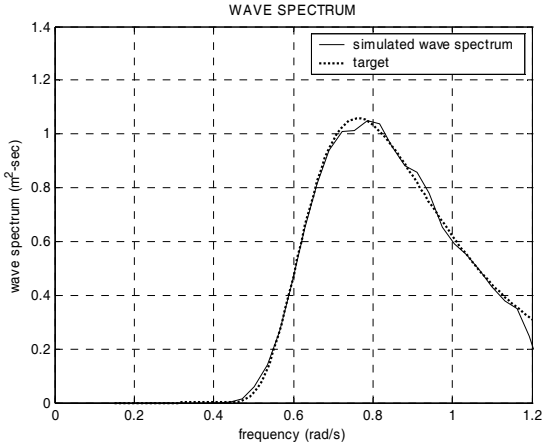

Fig. 10 Wave amplitude spectrum (side by side Case 2)

CASE 1 Co-linear Environment
(Hs=3.0m, Tp=16.5sec, Gamma=6.0)

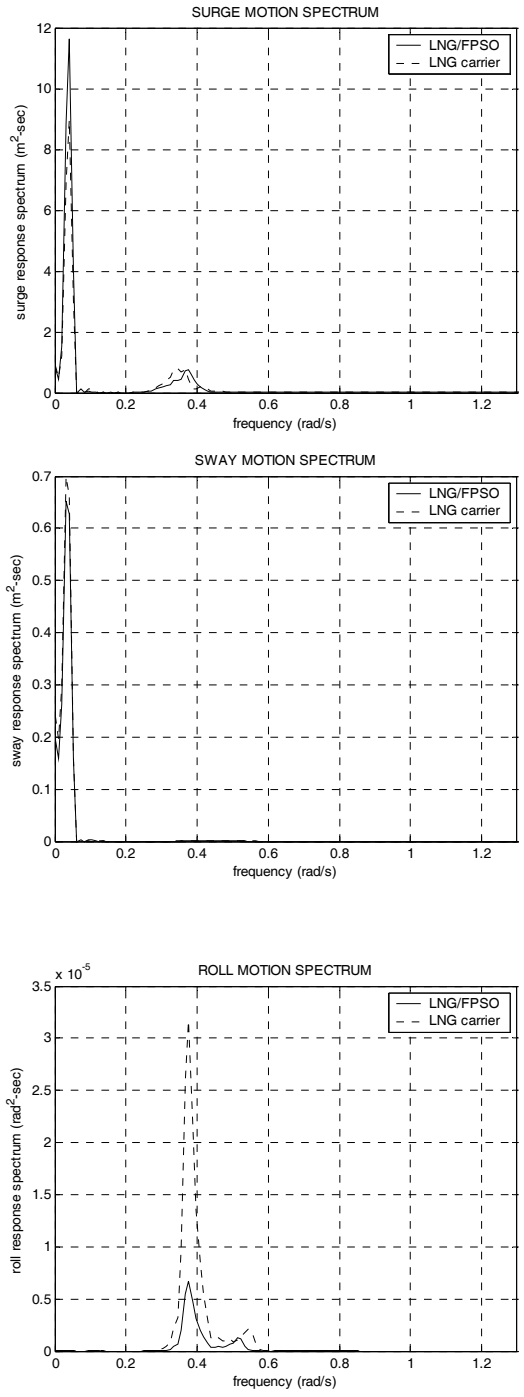

Fig. 11 Motion amplitude spectra (without hydrodynamic interaction CASE 1)

CASE 1 Co-linear Environment
(Hs=3.0m, Tp=16.5sec, Gamma=6.0)

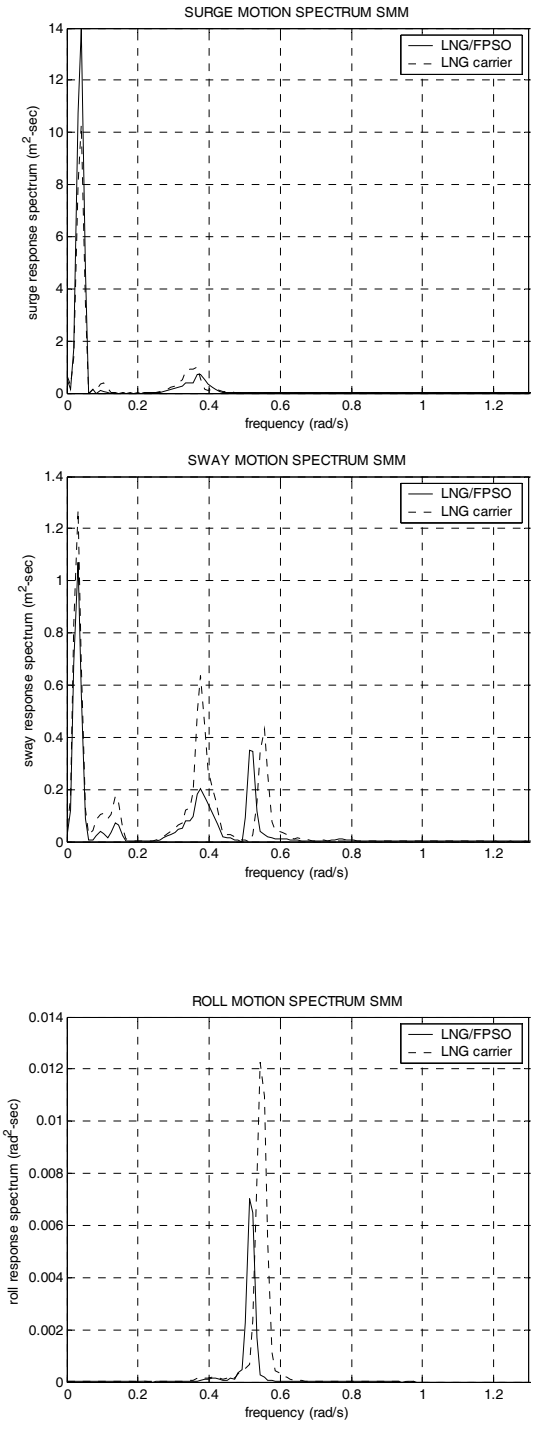

Fig 12. Motion amplitude spectra (SMM CASE 1)

CASE 1 Co-linear Environment
(Hs=3.0m, Tp=16.5sec, Gamma=6.0)

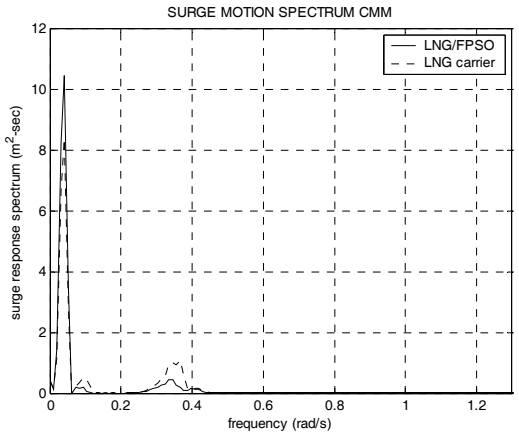

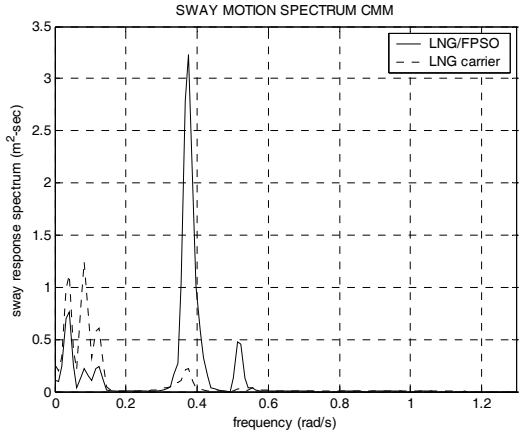

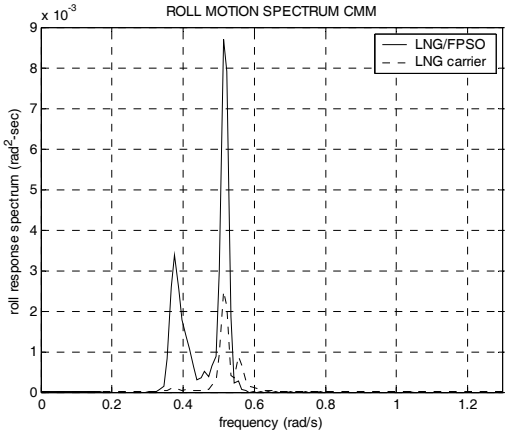

Fig 13. Motion amplitude spectra (CMM CASE 1)

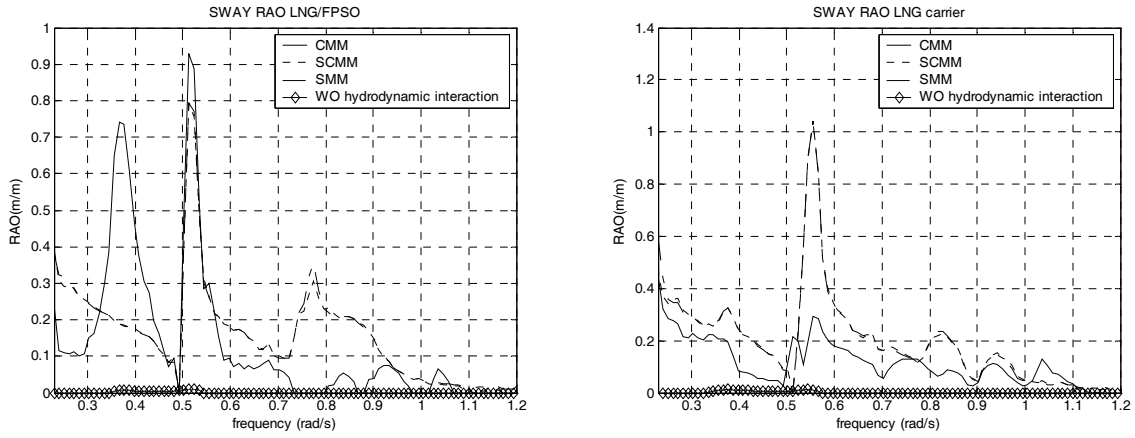

Fig. 14 Sway RAOs obtained from time-domain coupled analysis (side by side moored FPSO (or LNG Carrier) and Shuttle for Case 1)

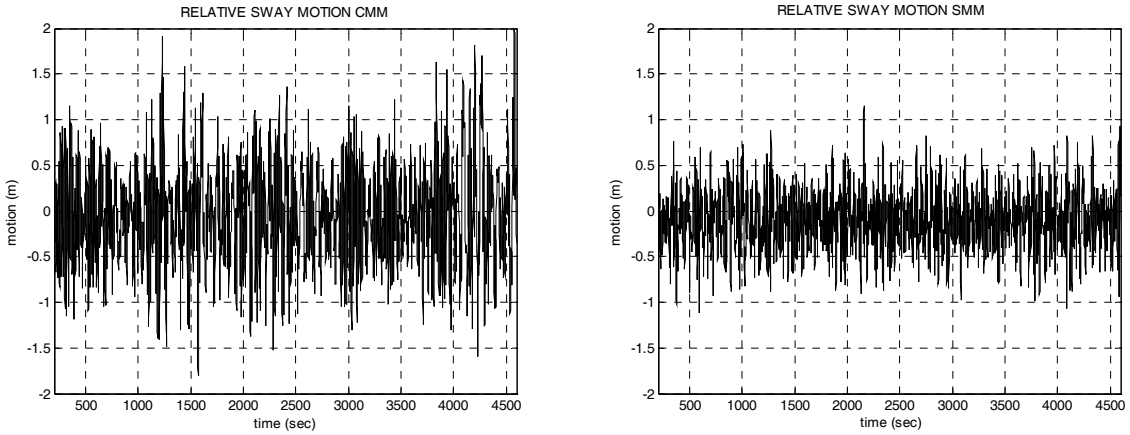

Fig. 15 Relative sway-motion time series (CASE 1)

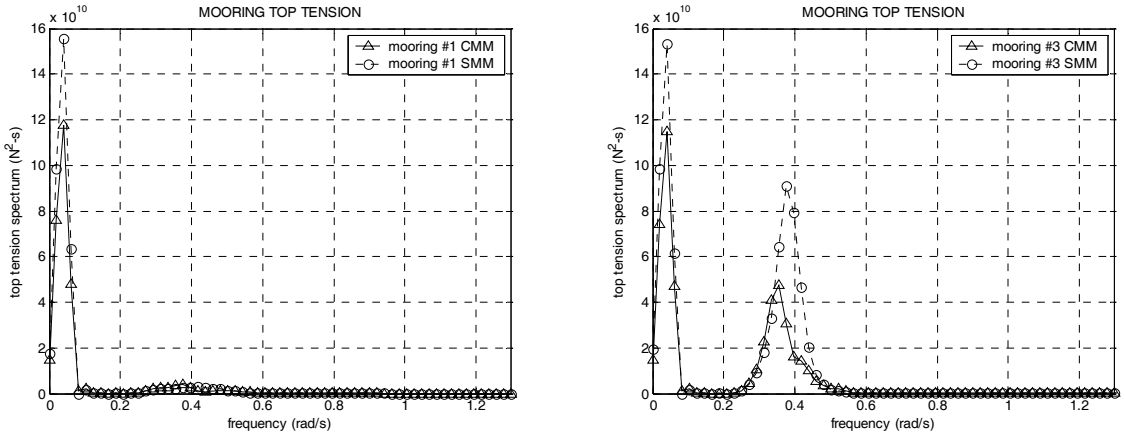

Fig. 16 Mooring top-tension spectra (Case 1)

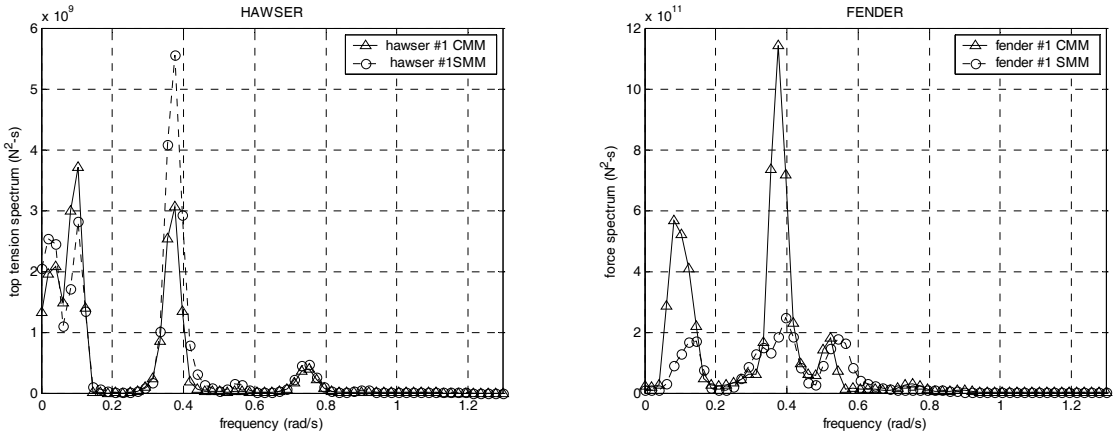

Fig. 17 Hawser top-tension and fender-force spectra (Case 1)

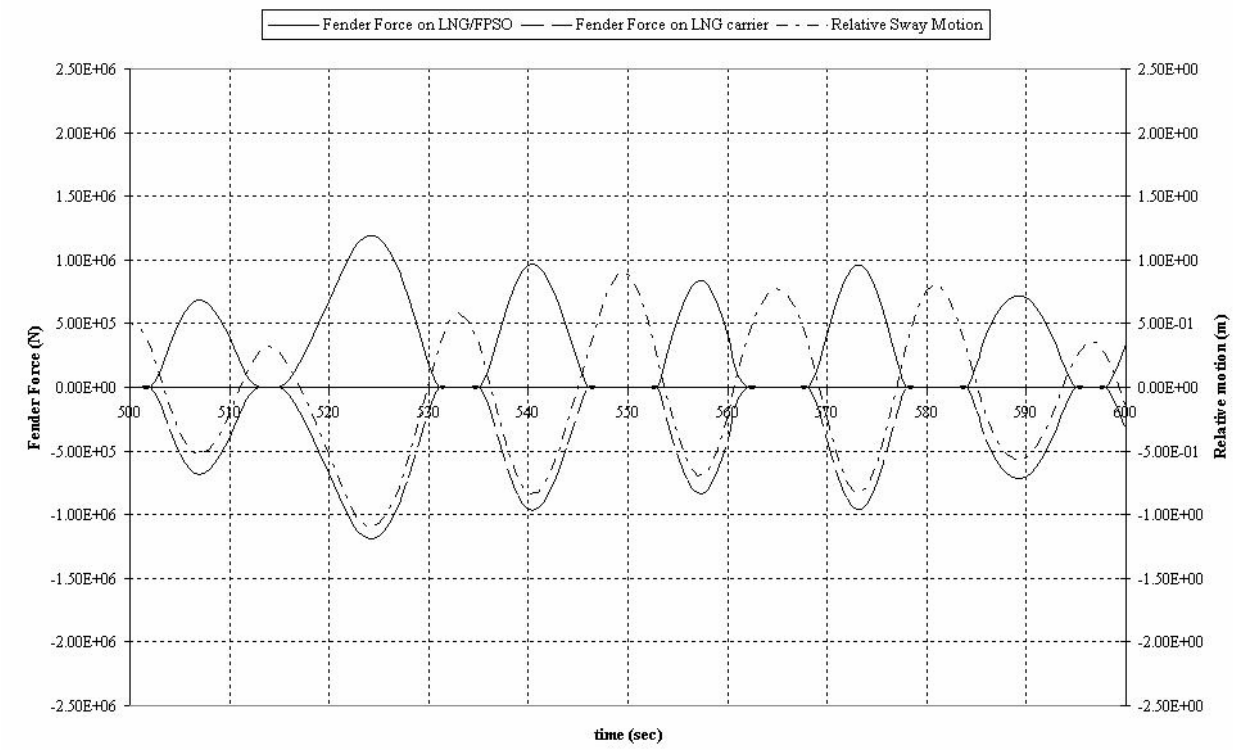

Fig. 18 Example of Fender force and relative sway motion (Case 1)

Figs. 19-23 (and Table 8-10) show the simulation results with 8.25-second (0.76 rad/sec) wave peak period (Case 2). The Case 2 wave spectrum, representing more fully-developed seas, is more wide-banded compared to Case 1. The sway results show that SMM gives higher maximum values (32% for the FPSO and 10% for the shuttle) compared to CMM. The FPSO (or LNG Carrier) roll-motion standard deviation from SMM is twice greater than that of CMM (see Table 8). As a result, its maximum is over-predicted by 52%. Fig. 21 shows the time histories of relative sway motions. The relative sway standard deviation and maximum are 12% and 32% over-predicted by SMM. In Figs 22,23, and Table 11, the spectra and statistics of mooring top-tension, hawser tension, and fender force are given. The mooring and hawser tension are slightly under-predicted but fender force is slightly over-predicted by SMM.

CASE 2 Co-linear Environment
(Hs=3.0m, Tp=8.25sec, Gamma=1.0)

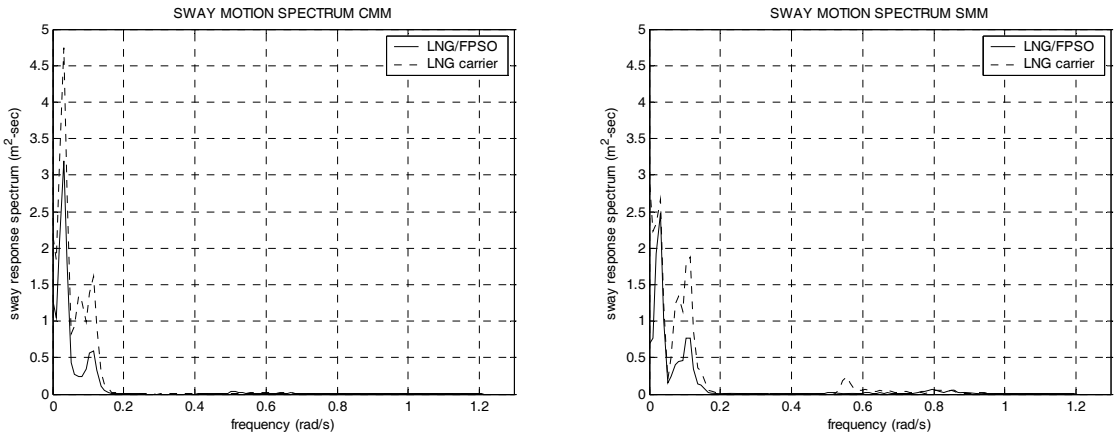

Fig. 19 Sway motion amplitude spectra (side-by-side moored FPSO (or LNG Carrier) and Shuttle for Case 2)

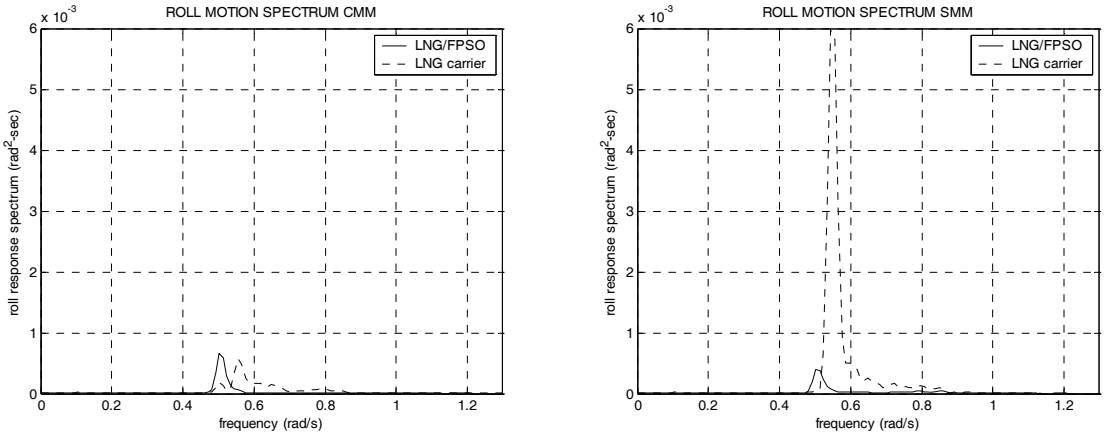

Fig. 20 Roll motion amplitude spectra (side-by-side moored FPSO (or LNG Carrier) and Shuttle for Case 2)

CASE 2 Co-linear Environment Relative Motion Time Series
(Hs=3.0m, Tp=8.25sec, Gamma=1.0)

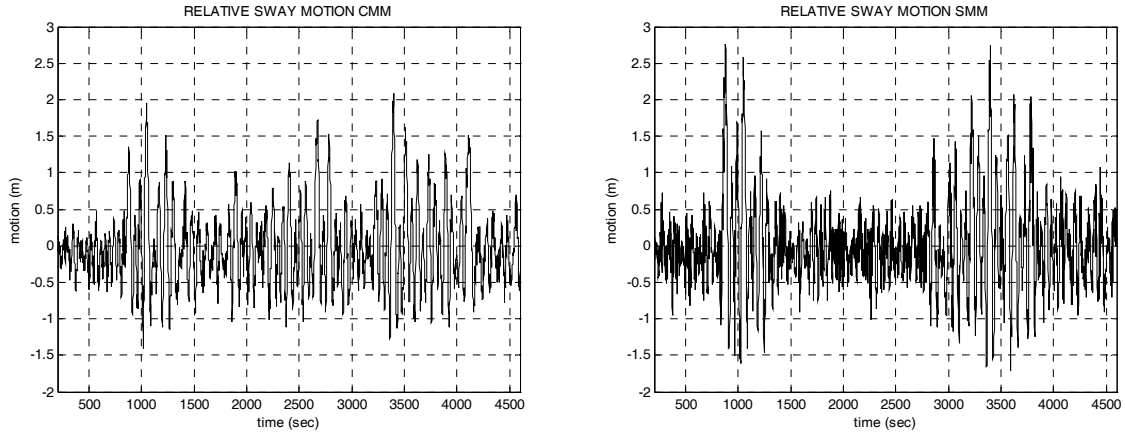

Fig. 21 Relative sway motion time series (side-by-side moored FPSO (or LNG Carrier) and Shuttle for Case 2)

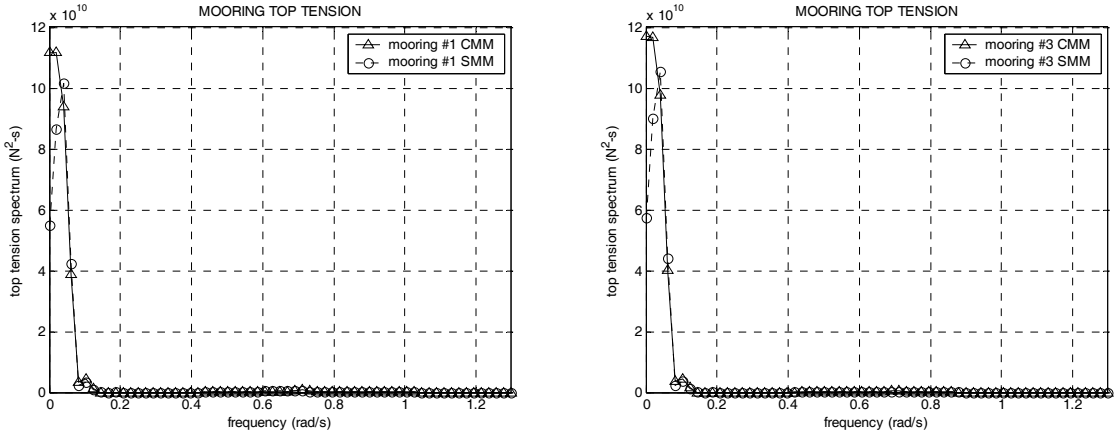

Fig. 22 Mooring top tension spectra (Case 2)

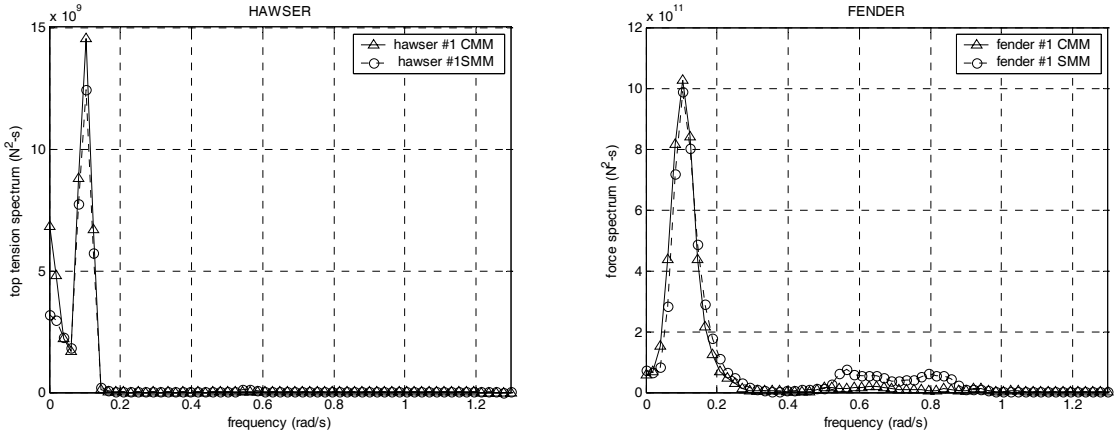

Fig. 23 Hawser top-tension and fender-force spectra (Case 2)

Table 4:Summary of motion statistics of side-by-side moored FPSO (or LNG Carrier) and Shuttle carrier (CASE 1)

		Combined Matrix Method						Separated Matrix Method					
		MEAN	MIN	MAX	STD	WF	LF	MEAN	MIN	MAX	STD	WF	LF
SURGE (m)	FPSO (or LNG Carrier)	-4.19E-01	-2.09E+00	1.40E+00	5.39E-01	1.86E-01	5.06E-01	-4.87E-01	-2.29E+00	1.55E+00	6.20E-01	2.28E-01	5.78E-01
	Shuttle	-1.66E-01	-1.93E+00	1.48E+00	5.45E-01	2.80E-01	4.68E-01	-1.24E-01	-1.99E+00	1.48E+00	5.76E-01	2.70E-01	5.10E-01
SWAY (m)	FPSO (or LNG Carrier)	2.96E-02	-1.12E+00	1.41E+00	4.13E-01	3.69E-01	1.87E-01	-5.17E-02	-9.19E-01	6.93E-01	2.40E-01	1.65E-01	1.73E-01
	Shuttle	7.16E-02	-1.30E+00	8.77E-01	3.13E-01	1.18E-01	2.90E-01	4.82E-02	-1.03E+00	1.15E+00	3.03E-01	2.22E-01	2.06E-01
HEAVE (m)	FPSO (or LNG Carrier)	-5.99E-01	-1.58E+00	4.53E-01	2.57E-01	2.56E-01	4.55E-03	-6.04E-01	-1.75E+00	7.33E-01	3.46E-01	3.46E-01	1.84E-02
	Shuttle	1.99E-03	-7.94E+00	7.92E+00	3.00E+00	3.00E+00	0.00E+00	2.19E-03	-7.41E+00	7.37E+00	2.81E+00	2.81E+00	0.00E+00
ROLL (deg)	FPSO (or LNG Carrier)	-2.36E-03	-3.86E+00	3.55E+00	1.17E+00	1.17E+00	1.59E-02	-1.34E-03	-2.18E+00	2.23E+00	8.33E-01	8.33E-01	1.94E-02
	Shuttle	-1.02E-02	-1.89E+00	1.96E+00	5.89E-01	5.89E-01	2.39E-02	-1.07E-02	-3.34E+00	3.22E+00	1.25E+00	1.25E+00	2.21E-02
PITCH (deg)	FPSO (or LNG Carrier)	2.08E-01	-5.14E-01	9.33E-01	1.95E-01	1.95E-01	1.30E-03	2.09E-01	-6.13E-01	1.14E+00	2.63E-01	2.63E-01	6.30E-03
	Shuttle	-2.25E-04	-4.21E+00	4.10E+00	1.59E+00	1.59E+00	0.00E+00	-3.26E-04	-3.88E+00	3.82E+00	1.47E+00	1.47E+00	0.00E+00
YAW (deg)	FPSO (or LNG Carrier)	2.78E-01	-5.36E-01	9.32E-01	2.49E-01	2.05E-01	1.42E-01	4.43E-01	-1.72E-01	9.54E-01	2.24E-01	4.83E-02	2.18E-01
	Shuttle	3.44E-01	-6.37E-01	1.09E+00	2.58E-01	1.21E-01	2.28E-01	5.24E-01	-4.14E-01	1.36E+00	2.86E-01	1.86E-01	2.18E-01

Table 5:Summary of relative-motion statistics of side-by-side moored FPSO (or LNG Carrier) and Shuttle (CASE 1)

	Combined Matrix Method				Separated Matrix Method		
	SURGE	SWAY	HEAVE		SURGE	SWAY	HEAVE
Unit	m	m	m		m	m	m
MAX	6.28E-01	1.98E+00	7.02E+00	MAX	7.04E-01	1.15E+00	6.81E+00
MIN	-1.01E+00	-1.81E+00	-8.23E+00	MIN	-1.30E+00	-1.12E+00	-8.23E+00
STD	2.55E-01	5.55E-01	2.88E+00	STD	3.25E-01	3.18E-01	2.84E+00

Table 6:Motion difference between Combined Matrix Method and Separated Matrix Method (Case 1)

		Difference					
		MEAN	MIN	MAX	STD	WF	LF
SURGE (m)	FPSO (or LNG Carrier)	6.73E-02	2.00E-01	-1.55E-01	-8.12E-02	-4.18E-02	-7.13E-02
	Shuttle	-4.28E-02	5.92E-02	-6.23E-03	-3.11E-02	9.97E-03	-4.17E-02
SWAY (m)	FPSO (or LNG Carrier)	8.14E-02	-1.99E-01	7.17E-01	1.74E-01	2.03E-01	1.34E-02
	Shuttle	2.34E-02	-2.76E-01	-2.75E-01	9.59E-03	-1.04E-01	8.35E-02
HEAVE (m)	FPSO (or LNG Carrier)	4.29E-03	1.70E-01	-2.79E-01	-8.96E-02	-8.92E-02	-1.39E-02
	Shuttle	-2.04E-04	-5.28E-01	5.50E-01	1.91E-01	1.91E-01	0.00E+00
ROLL (deg)	FPSO (or LNG Carrier)	-1.02E-03	-1.68E+00	1.32E+00	3.33E-01	3.34E-01	-3.51E-03
	Shuttle	4.76E-04	1.44E+00	-1.26E+00	-6.61E-01	-6.62E-01	1.79E-03
PITCH (deg)	FPSO (or LNG Carrier)	-1.50E-03	9.94E-02	-2.03E-01	-6.89E-02	-6.88E-02	-4.99E-03
	LNG carrier	1.01E-04	-3.28E-01	2.73E-01	1.16E-01	1.16E-01	0.00E+00
YAW (deg)	FPSO (or LNG Carrier)	-1.65E-01	-3.63E-01	-2.16E-02	2.59E-02	1.57E-01	-7.66E-02
	Shuttle	-1.79E-01	-2.22E-01	-2.73E-01	-2.78E-02	-6.45E-02	1.05E-02

Table 7:Summary of statistics of mooring and hawser top tension, and fender force (Case 1)

	Combined Matrix Method				Separated Matrix Method			
	MEAN (N)	MIN (N)	MAX(N)	STD (N)	MEAN (N)	MIN (N)	MAX(N)	STD (N)
Mooring 1	4.27E+06	4.01E+06	4.48E+06	7.66E+04	4.28E+06	3.99E+06	4.51E+06	8.65E+04
Mooring 2	4.19E+06	3.86E+06	4.51E+06	1.12E+05	4.20E+06	4.04E+06	4.39E+06	5.15E+04
Mooring 3	4.12E+06	3.83E+06	4.45E+06	9.84E+04	4.11E+06	3.69E+06	4.48E+06	1.22E+05
Mooring 4	4.20E+06	3.90E+06	4.48E+06	9.22E+04	4.18E+06	3.89E+06	4.46E+06	7.84E+04
Hawser 1	1.61E+06	1.55E+06	1.70E+06	2.25E+04	1.60E+06	1.53E+06	1.70E+06	2.53E+04
Fender 1	3.44E+05	0.00E+00	1.83E+06	3.62E+05	3.17E+05	0.00E+00	1.21E+06	2.47E+05

Table 8:Summary of motion statistics of side-by-side moored FPSO (or LNG Carrier) and Shuttle (CASE 2)

		Combined Matrix Method						Separated Matrix Method					
		MEAN	MIN	MAX	STD	WF	LF	MEAN	MIN	MAX	STD	WF	LF
SURGE (m)	FPSO (or LNG Carrier)	6.43E-01	-9.41E-01	2.44E+00	5.74E-01	2.74E-02	5.73E-01	6.27E-01	-7.16E-01	2.11E+00	5.31E-01	2.87E-02	5.30E-01
	Shuttle	-8.19E-01	-2.25E+00	8.38E-01	5.06E-01	4.15E-02	5.04E-01	-8.13E-01	-2.24E+00	7.16E-01	4.86E-01	4.52E-02	4.84E-01
SWAY (m)	FPSO (or LNG Carrier)	4.11E-01	-5.61E-01	1.49E+00	3.59E-01	5.65E-02	3.54E-01	4.18E-01	-6.32E-01	1.97E+00	3.46E-01	9.75E-02	3.32E-01
	Shuttle	4.26E-01	-1.30E+00	1.73E+00	5.01E-01	6.95E-02	4.96E-01	4.09E-01	-1.41E+00	1.91E+00	4.77E-01	1.40E-01	4.55E-01
HEAVE (m)	FPSO (or LNG Carrier)	-9.01E-01	-1.12E+00	-6.67E-01	6.81E-02	6.81E-02	1.02E-03	-9.01E-01	-1.11E+00	-6.85E-01	6.73E-02	6.73E-02	5.97E-04
	Shuttle	-5.30E-03	-2.18E-01	2.07E-01	5.41E-02	5.40E-02	4.19E-03	-5.27E-03	-1.86E-01	1.89E-01	5.20E-02	5.19E-02	3.53E-03
ROLL (deg)	FPSO (or LNG Carrier)	-4.91E-02	-9.04E-01	7.41E-01	2.95E-01	2.92E-01	3.94E-02	-4.91E-02	-1.10E+00	7.99E-01	2.89E-01	2.86E-01	3.91E-02
	Shuttle	6.43E-02	-1.58E+00	2.23E+00	4.18E-01	4.08E-01	8.80E-02	6.36E-02	-2.70E+00	3.40E+00	9.34E-01	9.30E-01	8.74E-02
PITCH (deg)	FPSO (or LNG Carrier)	3.11E-01	2.12E-01	4.16E-01	2.91E-02	2.91E-02	4.21E-04	3.11E-01	2.14E-01	4.15E-01	2.80E-02	2.80E-02	2.94E-04
	Shuttle	1.41E-04	-9.44E-02	9.98E-02	2.91E-02	2.91E-02	1.41E-03	9.40E-05	-1.46E-01	1.66E-01	3.57E-02	3.57E-02	1.06E-03
YAW (deg)	FPSO (or LNG Carrier)	-2.22E+00	-3.96E+00	-4.82E-01	8.39E-01	2.96E-02	8.38E-01	-2.18E+00	-3.46E+00	-5.01E-01	5.81E-01	5.26E-02	5.79E-01
	Shuttle	-2.15E+00	-3.97E+00	-2.89E-01	8.63E-01	4.84E-02	8.61E-01	-2.13E+00	-3.58E+00	-4.14E-01	6.21E-01	7.90E-02	6.16E-01

Table 9:Summary of relative motion statistics of side-by-side moored FPSO (or LNG Carrier) and Shuttle (CASE 2)

	Combined Matrix Method				Separated Matrix Method		
	SURGE	SWAY	HEAVE		SURGE	SWAY	HEAVE
Unit	m	m	m		m	m	m
MAX	2.91E+00	2.09E+00	-2.44E-01	MAX	2.74E+00	2.75E+00	-3.00E-01
MIN	-1.15E-01	-1.41E+00	-9.41E-01	MIN	2.93E-01	-1.71E+00	-8.75E-01
STD	6.49E-01	5.38E-01	9.57E-02	STD	4.99E-01	6.02E-01	7.84E-02

Table 10:Motion difference between Combined Matrix Method and Separated Matrix Method (Case 2)

		Difference					
		MEAN	MIN	MAX	STD	WF	LF
SURGE (m)	FPSO (or LNG Carrier)	1.62E-02	-2.25E-01	3.29E-01	4.28E-02	-1.32E-03	4.29E-02
	Shuttle	-5.55E-03	-1.44E-02	1.22E-01	1.93E-02	-3.67E-03	1.97E-02
SWAY (m)	FPSO (or LNG Carrier)	-6.52E-03	7.15E-02	-4.84E-01	1.26E-02	-4.11E-02	2.22E-02
	Shuttle	1.72E-02	1.08E-01	-1.76E-01	2.41E-02	-7.10E-02	4.05E-02
HEAVE (m)	FPSO (or LNG Carrier)	-1.91E-05	-2.55E-03	1.73E-02	7.92E-04	7.86E-04	4.27E-04
	Shuttle	-2.93E-05	-3.16E-02	1.79E-02	2.07E-03	2.03E-03	6.53E-04
ROLL (deg)	FPSO (or LNG Carrier)	-5.60E-06	1.94E-01	-5.77E-02	6.12E-03	6.15E-03	2.70E-04
	Shuttle	6.87E-04	1.12E+00	-1.17E+00	-5.16E-01	-5.22E-01	6.13E-04
PITCH (deg)	FPSO (or LNG Carrier)	-5.04E-06	-1.86E-03	1.18E-03	1.10E-03	1.10E-03	1.28E-04
	Shuttle	4.69E-05	5.18E-02	-6.60E-02	-6.57E-03	-6.59E-03	3.50E-04
YAW (deg)	FPSO (or LNG Carrier)	-4.45E-02	-4.94E-01	1.91E-02	2.58E-01	-2.30E-02	2.59E-01
	Shuttle	-2.10E-02	-3.89E-01	1.25E-01	2.42E-01	-3.06E-02	2.46E-01

Table 11:Summary of statistics of mooring and hawser top tension, and fender force (Case 2)

	Combined Matrix Method				Separated Matrix Method			
	MEAN (N)	MIN (N)	MAX(N)	STD (N)	MEAN (N)	MIN (N)	MAX(N)	STD (N)
Mooring 1	4.08E+06	3.83E+06	4.31E+06	8.11E+04	4.08E+06	3.87E+06	4.28E+06	7.52E+04
Mooring 2	4.10E+06	3.93E+06	4.25E+06	5.17E+04	4.10E+06	3.90E+06	4.25E+06	4.83E+04
Mooring 3	4.23E+06	3.99E+06	4.48E+06	8.25E+04	4.22E+06	4.03E+06	4.45E+06	7.62E+04
Mooring 4	4.21E+06	4.06E+06	4.38E+06	5.19E+04	4.21E+06	4.05E+06	4.43E+06	4.92E+04
Hawser 1	1.63E+06	1.55E+06	1.72E+06	2.99E+04	1.63E+06	1.55E+06	1.72E+06	2.73E+04
Fender 1	3.26E+05	0.00E+00	1.47E+06	3.11E+05	3.22E+05	0.00E+00	1.74E+06	3.30E+05

IV. SUMMARY and CONCLUSION

The safety and operability of side-by-side offloading operation is greatly influenced by the relative motions between adjacent vessels. Therefore, the accurate motion prediction of two vessels including all the hydrodynamic interactions with elastic lines is of great importance. The fender reaction force, which exhibits large force with contact but no force without contact, also plays a role in relative sway and yaw motions. This kind of fender-contact force can only be realized in time-domain simulations. The time-domain simulation of two vessels including all the hydrodynamic interactions, fender effects, and also the exact coupling effects with mooring lines, hawsers, and risers has never been published. This study presents such an original study for FPSO (or LNG Carrier) and Shuttle in side-by-side arrangement.

Nowadays, the offshore industry analyzes the relative motions between two vessels connected by lines by two typical approximation methods: (i) NHI: iteration method between two vessels without considering hydrodynamic interaction effects (ii) SMM: iteration method between two vessels with partially considering hydrodynamic interaction effects (ignoring the off-diagonal cross-coupling terms in 12x12 hydrodynamic coefficient matrix). In this study, an exact time-domain simulation method including all the 12x12 hydro-dynamic coefficients in a hull-line combined matrix is developed and called CMM. With this exact solution available, the performance of the two approximation methods were tested for various environmental conditions.

For side-by-side loading, vessel interactions are more important and the full hydrodynamic coupling between the vessels, i.e., the CMM should be used. The simpler approximations, SMM and NHI, can introduce appreciable errors and should be used with care. Numerical examples illustrated the differences between the CMM for two different environmental conditions (co-linear wind, wave, and current in head direction) illustrate that there may be large discrepancies between CMM and the approximation methods. The SMM is better than NHI but may still significantly over-predict or under-predict the actual relative motions, hawser and mooring tension, and fender forces. This means that even the cross-coupling (off-diagonal block) terms of the full hydrodynamic coefficient matrix play an important role in the case of side-by-side offloading operation. Therefore, such approximation methods should be used with care.

In the case of tandem offloading, the differences between full- coupling and the approximate methods are small.

This study was carried out in the context of potential theory, which is known to produce reasonable motion results except roll. The pumping mode in the gap caused negative added mass and large motions. Viscous effects and nonlinearity may further reduce the roll motions and the pumping mode. The discrepancy between the exact (CMM) and other approximation methods (SMM, NHI) may even be greater in non-parallel or beam-sea condition. Those will be the subjects of future study.

Acknowledgement

This research was financially supported by MMS (Minerals Management Service) and OTRC (Offshore Technology Research Center) industry consortium.

References

Arcandra, T. 2001. Hull/Mooring/Riser Coupled Dynamic Analysis of a Deepwater Floating Platform with Polyester Lines. Ph.D. Dissertation, Civil Engineering Department, Texas A&M University, College Station, TX.

Arcandra, T., Nurtjahyo, P. & Kim, M.H. 2002. Hull/Mooring/Riser Coupled Analysis of a Turret-Moored FPSO 6000 ft: Comparison between Polyester and Buoys-Steel Mooring Lines. Proc. 11th Offshore Symposium The Texas Section of the Society of Naval Architects and Marine Engineers, SNAME, 1-8.

Arcandra, T., Prahoro, N. and Kim, M.H. 2004 Effect of line dynamics and hull viscous drag on the motion of turret-moored FPSO. OMAE Specialy Conference on FPSO Integrity, Houston

Buchner, B., Dijk, A., and Wilde, J., 2001. Numerical Multiple-Body Simulations of Side-by-Side Mooring To a n FPSO. . Proc. 11th Int. Offshore and Polar Eng. Conference, ISOPE, 1, 343-353.

Choi, Y. R. and Hong, S. Y. 2002. An Analysis of Hydrodynamic Interaction of Floating Multi-Body Using Higher-Order Boundary Element Method. Proc. 12th Int. Offshore and Polar Eng. Conference, ISOPE, 1, 303-308.

Fang, M. C. and Kim, C. H. 1986. Hydrodynamically Coupled Motions of Two Ship Advancing in Oblique waves. Journal of Ship Research, 30 (3), 159-171.

Garrett, D. L., 1982. Dynamic analysis of slender rods. Journal Energy Resources Technology, vol. 104, pp. 302-307.

Hong, S. Y., Kim, J. H., Cho, S. K., Choi, Y. R., and Kim, Y. S., 2003. Numerical and Experimental Study on Hydrodynamic Interaction of Side-by-Side Moored Multiple Vessels. Proc. of Deep Water Mooring System, ASCE, 198-215.

Huijsmans, R. H. M., Pinkster, J. A., and de Wilde, J. J. 2001. Diffraction and Radiation of Waves Arround Side-by-Side Moored Vessels. Proc. 11th Int. Offshore and Polar Eng. Conference, ISOPE, 1, 406-412.

Kim, M.H., Arcandra, T. & Kim, Y.B. 2001a. Validability of Spar Motion Analysis against Various Design Methodologies/Parameters. Proc. 20th Offshore Mechanics and Arctic Eng. Conference, OMAE01-OFT1063 [CD-ROM], L.A., Califonia.

Kim, M.H., Arcandra, T. & Kim, Y.B. 2001b. Validability of TLP Motion Analysis against Various Design Methodologies/Parameters. Proc. 11th Int. Offshore and Polar Eng. Conference, ISOPE, 3, 465-473.

Kim, M.H. and Kim, Y.B. 2002 Hull-mooring-riser coupled dynamic analysis of a tanker-based turret-moored FPSO in deep water Proc. 12th Int. Offshore and Polar Eng. Conference, ISOPE02

Kim, M.H., Koo, B.J., Mercier, R.M., and Ward, E.G. 2005. Vessel-mooring-riser coupled dynamic analysis of a turret-moored FPSO compared with OTRC experiment. J. of Ocean Engineering, Vol.32, pp1780-1802

Kim, Y.B. 2003. Dynamic Analysis of Multiple-Body Floating Platforms Coupled with Mooring Lines and Risers. Ph.D. Dissertation, Civil Engineering Department, Texas A&M University, College Station, TX.

Kodan, N. 1984. The Motion of Adjacent Floating Structure in Oblique Waves. Proc. 3rd Offshore Mechanics and Arctic Eng. Conference, OMAE, New Orleans, 1. 206-213

Koo, B. J., Kim M. H., and Randall, R. E. 2004. The Effect of Nonlinear Multi-contact Coupling with Gap between Risers and Guide Frames on Global Spar Motion Analysis. J. of Ocean Engineering. 31/11-12 pp. 1469-1502

Koo, B. J. and Kim M. H. 2005 Motion Analysis of Two Floating Platform with Mooring and Hawser Lines in Tandem Moored Operation by Combined Matrix Method and Separated Matrix. J. of Ocean Engineering and Technology. Vol.19, pp. 1-15

Lee D. H. 2002 Nonlinear Stability Analysis and Motion Control of Tandem Moored Tankers. Ph.D. Dissertation, Naval Architecture and Ocean Engineering, Seoul National University, Seoul.

Lee, C.H., 1999. WAMIT theory manual. Department of Ocean Engineering. MIT, MA

Lee, D.H. and Choi, H.S. 2000. A dynamic analysis of FPSO-shuttle tanker system. Proc. 10th Int. Offshore and Polar Eng. Conference, ISOPE, Vol.1, 302-307.

Loken A.E. 1981. Hydrodynamic Interaction between Several Floating Bodies of Arbitrary form in Waves. Proc. of Int'l Symposium on Hydrodynamics in Ocean Engineering, NIT, Trondhiem, 2. 745-779

Ma, W., Lee, M. Y., Zou, J., and Huang, E. W., 2000. Deepwater nonlinear coupled analysis tool. Offshore Technology Conference, (OTC 12085), Houston, TX.

OCIMF. 1994. Prediction of Wind and Current Loads on VLCCs. 2nd Edition, Witherby & Co. Ltd, London, England.

Ohkush, M. 1974. Ship Motions in Vicinity of a Structure. Proc. of Int'l Conf. on Behavior of Offshore Structure, NIT, Trondheim, 1. 284-306

Paulling, J.R., and Webster, W.C., 1986. A consistent large-amplitude analysis of the coupled response of a TLP and tendon system. Proceeding of the 5th Offshore Mechanics and Arctic Engineering Symposium, Vol. 3, pp.126-133.

Sphaier, S.H., Fernandes,A.C., and Correa,S.H. 2000. Maneuvering model for the FPSO horizontal plane behavior. Proc. 10th Int. Offshore and Polar Eng. Conference, ISOPE, Vol.1, 337-344

Van Oortmerssen, G. 1979. Hydrodynamic Interaction between Two Structures of Floating in Waves. Proc. Boss '79. 2nd Int'l Conf. on Behavior of Offshore Structure, London, 339-356

Wichers, J.E.W, Voogt, H.J., Roelofs, H.W. & Driessen, P.C.M. 2001b. DeepStar-CTR 4401- Benchmark Model Test. Technical Rep. No. 16417-1-OB, MARIN, Wageningen, Netherlands.

Wichers, J.E.W. & Develin, P.V. 2001a. Effect of Coupling of Mooring Lines and Risers on the Design Values for a Turret Moored FPSO in Deep Water of the Gulf of Mexico. Proc. 11th Int. Offshore and Polar Eng. Conference, ISOPE, 3, 480-487.

Wichers, J.E.W. 1988. A Simulation Model for a Single Point Moored Tanker. Ph.D. Dissertation, Delft University of Technology, Delft, The Netherlands

Table 12: Unit Conversion Table

Conversion Factors for Different Units of Measurements			
Quantity	**SI Unit**	**Other Unit**	**Inverse Factor**
Length	1m	3.281 feet (ft)	0.3048 m
	1 km	0.540 nautical miles	1.852 km
	1 km	0.6213712 mile	1.609344 km
Area	1 m^2	10.764 ft^2	0.0929m^2
Volume	1 m^3	35.315 ft^3	0.0283 m^3
	1 m^3	264.2 gallon (US)	0.00379 m^3
	1 m^3	220.0 gallon (UK)	0.00455 m^3
	1 m^3	6.29 barrel (US Petroleum)	0.1589 m^3
Velocity	1 m/s	3.281 ft/s	0.305 m/s
	1 m/s	1.943 knot	0.515 m/s
	1 m/s	2.2369 mph	0.44704 m/s
	1 km/hr	0.62137 mph	1.6093 km/hr
Mass	1 kg	2.205 pound	0.454 kg
	1 Mg	0.984 ton (long)	1.016 Mg
	1 Mg	1 tonne (metric)	1 Mg
Force	1 N	0.225 pound force	4.448 N
	1 MN	100.4 ton force	9964 N
	1 MN	224.81 kip	4448 N
	1 kg-force	0.0022046 kip	453.592 kg-force
Pressure	1 N/m^2	0.000145 psi	6895 N/m^2
	1 kg-force/cm^2	0.01422 ksi	70.307 kg-force/cm^2
	1 MN/m^2	20.885 kip/ft^2	47880 N/m^2
Energy	1 J	0.738 foot pounds	1.356 J
Power	1 W	0.00134 horsepower	745.7 W
Temperature	0^0 Celsius	32^0 Fahrenheit	-17.78^0 Celsius
Frequency	1 cycle/s	1 hertz	1 cycle/second
Flow Rates	1 m^3/day	6.289 barrel/day	0.1589 m^3/day
	1 m^3/day	35.3146 ft^3/day	0.0283 m^3/day
Density	1 g/cm^3	0.578 oz./$inch^3$	1.73 g/cm^3